Virus Research 267 (2019) 49–58

Contents lists available at ScienceDirect

Virus Research

journal homepage: www.elsevier.com/locate/virusres

AcMNPV-miR-3 is a miRNA encoded by Autographa californica nucleopolyhedrovirus and regulates the viral infection by targeting *ac101*

Yingzhen Jiao, Jinwen Wang*, Riqiang Deng, Xinghua Yu, Xunzhang Wang*

School of Life Science, Sun Yat-Sen University, Guangzhou, 510275, China

ARTICLE INFO

Keywords:
Baculovirus
AcMNPV
miRNA
AcMNPV-miR-3
Regulation
ac101

ABSTRACT

MicroRNAs (miRNAs), which are small noncoding RNAs found in plants, animals, and many viruses, regulate various biological processes. Our group has previously reported the first miRNA encoded by Autographa californica multiple Nucleopolyhedrovirus (AcMNPV), AcMNPV-miR-1, which regulates the expression of three viral genes. This study characterizes another miRNA encoded by AcMNPV, AcMNPV-miR-3. This miRNA is located on the opposite strand of the viral gene *ac101* coding sequence in the AcMNPV genome, and it can be detected at 6 h post-infection and accumulated to a peak around 12 h post-infection in AcMNPV infected Sf9 cells. Five viral genes (*ac101*, *ac23*, *ac25*, *ac86*, and *ac98*) were verified to be regulated by AcMNPV-miR-3. *Ac101* was markedly down-regulated by AcMNPV-miR-3 that may be via a siRNA-like cleavage mode. Administrating excessive AcMNPV-miR-3 resulted in decreased production of infectious budded virions (BV) and accelerated the formation of occlusion-derived virions (ODV). These results suggest that AcMNPV-miR-3 may play a regulatory role in BV and ODV production.

1. Introduction

Baculoviruses are rod-shaped viruses with circular double-stranded DNA genomes of 90 kb-180 kb. They are divided into four genera, namely, *Alphabaculovirus*, *Betabaculovirus*, *Gammabaculovirus*, and *Deltabaculovirus*, according to the insect hosts they were isolated from and their biological characteristics (Jehle et al., 2006). *Autographa californica multiple Nucleopolyhedrovirus* (AcMNPV) is the archetypal species of the *alphabaculovirus*. During the infection cycle, it produces two structurally and functionally distinct enveloped virion phenotypes which have distinct roles in viral pathogenesis: budded virus (BV) and occlusion derived virus (ODV) (Rohrmann, 2013). These virons are similar in their nucleocapsid structure but differ in the origin and composition of their envelopes and their roles in the virus life cycle.

MiRNAs are small noncoding RNAs that play critical roles in regulating various biological processes, such as growth, development, apoptosis, and immunoreaction (Bartel, 2004; Dong et al., 2013). So far viruses in several families have been shown to encode miRNAs, and viral miRNA identification and functional understanding continues to grow (Giudice et al., 2016; Kincaid and Sullivan, 2012). Virus-encoded miRNAs have been taken into account to influence viral replication and pathogenic potential through their regulation of viral gene expression or host gene expression (Hussain and Asgari, 2014; Skalsky and Cullen, 2010). Nevertheless, a limited number of studies on baculovirus miRNA have been carried out to understand their function. For example, BmNPV-miR-1 suppresses its host microRNA biogenesis by regulating Exportin-5 Cofactor Ran and increases the BmNPV load in infected larvae (Singh et al., 2012, 2010). BmNPV-miR-3 facilitates BmNPV infection by modulating the expression of *p6.9* and other late genes in *Bombyx mori* (Singh et al., 2014). AcMNPV-miR-1 is considered to target and down-regulate the expression of viral gene *odv-e25*, accelerate polyhedra formation, and promote viral infection efficiency in Trichoplusia ni larvae (Zhu et al., 2016, 2013).

In this study, AcMNPV-miR-3, another miRNA encoded by AcMNPV, was identified and characterized. It was located on the opposite strand of the viral gene ac101, indicating that ac101 is its primary target gene. Our results also confirmed that ac101 was down-regulated markedly by miR-3. Many studies have reported that binding of miRNAs to the coding sequence (CDS) of their target mRNAs with high complementarity could function similar to small interfering RNA associated with RNA silencing to guide sequence-specific cleavage in a developmentally controlled manner (Llave et al., 2002). Previous studies have shown that *ac101* is a core gene that is not only essential for BV and ODV production but also plays a vital role in viral infectivity and virus-induced nuclear actin polymerization (Braunagel et al., 2001; Li et al., 2010; Wang et al., 2015; Zhang et al., 2018). Considering this,

* Corresponding authors.
E-mail addresses: wangjinw@mail.sysu.edu.cn (J. Wang), wxz@mail.sysu.edu.cn (X. Wang).

https://doi.org/10.1016/j.virusres.2019.05.004
Received 20 December 2018; Received in revised form 4 May 2019; Accepted 7 May 2019
Available online 08 May 2019
0168-1702/

we focused our study on mainly how miR-3 regulates *ac101*.

2. Materials and methods

2.1. Viruses, cells, and insects

Sf9 (*Spodoptera frugiperda* IPLB-Sf21-AE clonal isolate 9) insect cells were cultured in Graces' medium supplemented with 10% fetal bovine serum at 27 °C. Human embryonic kidney cells (HEK293 cell line) were cultured in Dulbecco's Modified Eagle's Medium (DMEM) supplemented with 10% fetal bovine serum at 37 °C in a 5% CO_2 incubator. AcMNPV strain E2 accompanying the Bac-to-Bac® Baculovirus Expression System from Invitrogen was used in this study.

2.2. RNA isolation

Total RNA was isolated from approximately 10^7 infected cells harvested using Trizol agent (Invitrogen, USA) according to the manufacturer's protocol. Total RNA was dissolved in 50 µl RNase-free H_2O. The RNA solutes were digested for 30 min at 37 °C with RNase-free DNase I (TaKaRa) to remove any contaminating genomic DNA. RNA integrity was analyzed by gel electrophoresis using a 1% agarose gel alongside an RNA marker.

2.3. miRNA prediction and miRNA target prediction

AcMNPV encoded miRNAs were predicted through the same way as previously described (Zhu et al., 2013). Solexa sequencing of RNA samples was performed by Beijing Genomics Institute Shenzhen Co. (BGI-Shenzhen, China). Groups of Sf9 cells were infected with AcMNPV at a multiplicity of infection (MOI) of 10, and subsequently, RNA samples at 6, 12, and 24 h post infection (h p.i.), and mock-infected cells were extracted according to the manufacturer's protocol. The samples were sent to BGI for sequencing using Solexa technology, and 18–30 nucleotides (nt) fragments were sequenced. After removing the adaptor sequences from the raw data, the clean reads were analyzed, and four small RNA libraries were generated. All data have been uploaded to the SRA database (NCBI SRA accession number is PRJNA523298).

At the same time, we used the Vmir (Grundhoff et al., 2006) software to scan the AcMNPV genome (accession number NC_001623) in both orientations for sequences of 50–120 nt in length with characteristics of folding into stem-loop structures. In addition, these candidate segments were validated by using two online Web servers, MiPred (Jiang et al., 2007) and CSHMM (Agarwal et al., 2010). Finally, these small RNA reads in each small RNA library were mapped to the candidate segments by using the SOAP program (Li et al., 2009), and the candidates without matched reads were removed. The secondary structure of the pre-miR-3 was predicted using the RNAfold web server (http://rna.tbi.univie.ac.at/cgi-bin/RNAWebSuite/RNAfold.cgi), and the mfold web server (http://unafold.rna.albany.edu/?q=mfold/RNA-Folding-Form).

To predict the miR-3 target genes of the AcMNPV, the AcMNPV genome sequence (GenBank accession number NC_001623) was employed with three independent computational algorithms, TargetScan 5.1 (http://www.targetscan.org), miRanda (http://www.microrna.org/), and Pictar (http://pictar.mdc-berlin.de/). Then, the top seven candidate target genes were obtained after selection of the miR-3 seed region for further study.

2.4. miRNA mimic and miRNA inhibitor transduction in AcMMPV infected Sf9 cells

Nowadays, miRNA mimics and inhibitors provide a means to study the function of specific miRNAs in a range of organisms and to validate their role in regulating target genes. The miRNA mimics are small, double-stranded RNA molecules, designed to mimic endogenous mature miRNA molecules when transported into cells. In this study, a synthesized miR-3 mimic (5′-GCGGCGUAGG CUGCGCGGAC GCU-3′) (RIBOBIO, Guangzhou, China) was performed for miR-3 gain-of-function studies. In the meantime, a miRNA mimic with sequence based on *Caenorhabditis elegans* miRNA (Cel-miR-239b-5p, 5′-UUUGUACUAC ACAAAAGUAC UG-3′) (RIBOBIO, Guangzhou, China) was invoked as a negative control. On the contrary, miRNA inhibitors with chemical modification are steric blocking oligonucleotides that hybridize to mature miRNAs, and they are generally used to block the binding of miRNA and its target. A sequence-specific micrOFF™ miRNA inhibitor of miR-3 was synthesized based on the mature miR-3 reverse complement sequence (5′-AGCGUCCGCG CAGCCUACGC CGC-3′) (RIBOBIO, Guangzhou, China) for loss-of-function studies.

A total of 1×10^5 to 3×10^5 Sf9 cells in 0.5 mL of complete growth medium were plated in a 12-well plate. Then, the grouped Sf9 cells were transfected with 50 nmol/L (nM) Cel-miR-239b-5p mimic, 50 nM miR-3 mimic, or 100 nM miR-3 inhibitor oligonucleotides using Lipofectamine® RNAi MAX Transfection Reagent (Invitrogen, USA) according to the manufacturer's protocol. After that, all the transducted Sf9 cells were infected with AcMNPV (MOI of 1 or 10 for different downstream experiments) at 8 h posttransfection (h p.t.).

2.5. qRT-PCR

SYBR green-based quantitative reverse transcription PCR (qRT-PCR) was performed to define the expression profile of miRNA and its target genes. The stem-loop qRT-PCR method is widely used to detect and quantify mature miRNAs (Chen et al., 2005). For miRNA cDNA synthesis, RNA was reverse transcribed using the miRNA reverse transcription kit (TAKARA) in combination with the stem-loop reverse transcription primer (5′-GTCGTATCCA GTGCAGGGTC CGAGGTATTC GCACTGGATA CGACTTCCTT A-3′) according to the manufacturer's protocol. The 5S rRNA was reverse transcribed by using a random primer (Takara) and included as a reference of the respective sample. The qRT-PCR data for each sample were analyzed by using the $2^{-\triangle\triangle CT}$ method. Once the values for all the three experiments were recorded, a two-tailed student's *t*-test was performed to calculate the statistical significance of the results.

2.6. Northern blot

Northern blot hybridization with antisense oligonucleotides specific for AcMNPV-miR-3 was performed as previously described (Kim et al., 2010). The 23-nt long probe (5′-AGCGUCCGCG CAGCCUACGC CGC-3′) for AcMNPV-miR-3 was labeled with digoxin on its 5′-end. Total RNAs (20 µg) were separated on 7 M urea-denaturing 15% polyacrylamide gels, and siRNA Ladder Marker (TAKARA, Code No. 3430) was used as a molecular size marker.

2.7. Dual-luciferase reporter assay

Nowadays, the dual-luciferase reporter assay has been widely used as a tool to study gene transcription and regulation (Miranda et al., 2006; Svoboda, 2015). It is performed by sequentially measuring the Firefly luciferase (Fluc) and Renilla luciferase (Rluc) activities of the same sample, and the Fluc activity is measured as an endogenous transfection control to normalize the transfection efficiency. The psiCHECK™-2 Vector (psiCHECK2, GenBank® Accession Number AY535007, Promega Corporation) was designed to provide quantitative and rapid optimization of dual-luciferase reporter assay. The predicted miR-3 target sequences (*ac10*, *ac23*, *ac25*, *ac86*, *ac98*, *ac101*, and *ac126*) with the sticky ends of NotI and XhoI restriction enzyme sites were gained from annealing of long primers (˜60 bp containing the miRNA binding site and some flanking sequences, synthesized by Sangon Biotech, Shanghai, China). Each of the target DNA fragments

was cloned into the psiCHECK2 vector downstream of the *Renilla* translational stop codon. *Bombyx mori Actin 3* (A3) gene, an unspecific target of miR-3, was inserted into psiCHECK2 as a negative control, and the psiCHECK2 was invoked as a no-insert control. All the primer sequences are shown in Supplementary Table 1 and all constructs were sequenced to confirm the correct insertion.

The day before transfection, the HEK293 cells were plated in 48-well plates at a density of 2*10ˆ4 cells/well in 0.2 mL of complete growth medium. Each constructed plasmid was cotransfected along with 50 nM miR-3 mimic using Lipo2000™ (Invitrogen) according to the manufacturer's recommendations. A total of 50 nM Cel-miR-239b-5p mimic were also cotransfected with each plasmid as the negative control. Cells were lysed at 48 h after transfection and the luciferase activity was measured using the dual-luciferase reporter assay system (Promega) in a 96-well plate format according to the manufacturer's guidelines. Luciferase activities were measured using a GloMax®-Multi Microplate Multimode Reader (Promega Corporation, USA). The firefly luciferase enzyme activity was normalized to the Renilla luciferase enzyme activity, yielding the relative luciferase expression. The Rluc/Fluc ratio of cells cotransfected with the construct of interest was compared to that of cells transfected only with psiCHECK2 (used as a no-insert control, set at 1.0). Means that, Rluc/Fluc relative activities were finally normalized to the Rluc/Fluc values of the cells transfected by psiCHECK2. All measurements were taken in triplicate, and the values were normalized to the *Renilla* luciferase activity. The results are presented as the mean ± SD.

2.8. BV titer analysis

TCID50 end-point dilution in Sf9 cells was used to determine if infectious BV were produced as previously described (Lo and Chao, 2004), with some modifications (Lo and Chao, 2004). The BV titers were determined in triplicate using a 50% tissue culture infective dose ($TCID_{50}$) end-point dilution assay in Sf9 cells. The dilution of the virus at which 50% of the cell cultures are infected can be calculated and expressed as the 50% infectious dose per milliliter. Briefly, Sf9 cells were infected with AcMNPV (MOI of 1) 8 h after transfection by the miR-3 mimic, miR-3 inhibitor, or Cel-miR-239b-5p mimic. At the indicated time points, the supernatants containing the BVs were harvested, and cell debris was removed by centrifugation (3000 × g for 10 min). Subsequently, all the samples were tested by a $TCID_{50}$ end point dilution assay with three replications.

2.9. Electron microscopy analysis

Transmission electron microscopy (TEM) was performed to monitor the morphological events. Infected Sf9 cells were treated and prepared for electron microscopy as described previously (Li et al., 2005). The samples were observed under a JEM-100CX-II transmission electron microscope at an accelerating voltage of 120 kV.

2.10. Construction of miR-3 overexpression baculovirus

To evaluate the miR-3 function, gain-of-function and loss-of-function experiments were performed using recombinant baculovirus with miR-3 precursor and miR-3 sponges. The microRNA "sponge" method was developed by Ebert et al. as a means to create continuous miRNA loss-of-function (Ebert et al., 2007). Herein, miR-3 sponges with tandem eight repeated miRNA antisense sequences were expected to interact with the mature miRNA by sequestering miRNAs from endogenous targets, and their effectiveness was comparable to antisense oligonucleotides.

Recombinant baculovirus $v^{Ac-miR-3-GP}$, $v^{Ac\text{-}miR\text{-}3\text{-}sponge\text{-}GP}$, $v^{Ac\text{-}NC\text{-}GP}$, and $v^{Ac\text{-}WT\text{-}GP}$ were constructed by the Bac-to-Bac system according to the manufacturer's protocol (Thermo Fisher Scientific). The donor plasmids (pFB-miR-3-GP, pFB-miR-3-sponge-GP, and pFB-NC-GP) were constructed based on pFB-GP plasmid (constructed by our group member Li et al. (2005), based on pFastBac1 backbone, and inserted the polyhedrin and green fluorescent protein genes). To gain pFB-miR-3-GP, eight copies of AcMNPV-miR-3 precursor with some flanking sequences were tandemly inserted downstream of the ie-1 promoter and upstream of the SV40 poly (A) sequence via isocaudomers of Bgl II (A|GATCT) and BamH I (G|GATCC). A nonrelated artificial stem-loop structure was used as a negative control (NC), and the sequence was inserted to construct pFB-NC-GP donor plasmid with ie-1 promoter and SV40 poly (A) tail. Whereas, an artificial microRNA sponge was constructed by inserting eight tandem-arrayed bulged miR-3 binding sites into the pFB-GP plasmid with ie-1 promoter and SV40 poly (A) tail to achieve miR-3 loss-of-function. All constructs were sequenced to confirm the correct insertion. After that, donor plasmids were transfected into DH10B competent cells containing the bMON14272 bacmid and the helper plasmid pMON7124, respectively. Then, positive clones of $v^{Ac-miR-3-GP}$, $v^{Ac\text{-}NC\text{-}GP}$, $v^{Ac\text{-}miR\text{-}3\text{-}sponge\text{-}GP}$, and $v^{Ac\text{-}WT\text{-}GP}$ were selected using blue/white screening and confirmed by PCR method.

2.11. Statistical analysis

All experiments had proven to be reproducible. In most experiments, we performed one-way analyses of variance (ANOVA) with Dunnett's tests comparing each of the treatment group mean with the mean of the control group. In qRT-PCR and luciferase assays, comparisons were performed with Student's *t*-test to determine statistical significance.

3. Results

3.1. Prediction of AcMNPV- miR-3

It was predicted that the AcMNPV-miR-3 precursor is 67-nt in length and located at (+) 87727- (+) 87794 of the AcMNPV genome, that is, on the negative strand of the core gene ac101 CDS (Fig. 1A). AcMNPV-miR-3 precursor sequence was analyzed to study its conservation in baculovirus via an alignment of pre-miR-3 DNA sequences from AcMNPV, Plutella xylostella multiple nucleopolyhedrovirus (PlxyMNPV), Bombyx mori nucleopolyhedrovirus (BmNPV), Rachiplusia ou nucleopolyhedrovirus (RaouMNPV), and Thysanoplusia orichalcea nucleopolyhedrovirus (ThorNPV). The results showed that AcMNPV-miR-3 miRNA was not highly conserved among baculovirus genomes (see Supplementary Fig. 1). The secondary structure of the AcMNPV-miR-3 precursor was predicted using the RNAfold web server and the mfold web server, and the possible secondary structure is shown in Fig. 1B, in with the 23-nt long mature AcMNPV-miR-3 is highlighted.

3.2. Identification of AcMNPV-miR-3 in AcMNPV-infected Sf9 cells

Northern blot and qRT-PCR were performed to investigate AcMNPV-miR-3 expression in AcMNPV infected Sf9 cells. The northern blot was performed for precise detection of miR-3 expression in AcMNPV infected Sf9 cells with a 5′-end digoxin labeled probe for mature miR-3. Following consideration of the low copy number of miR-3 in deep sequencing results, approximately 20 μg total RNA samples were loaded for miR-3 detection in northern blot analysis. As shown in Fig. 2A, approximately 23 nt bands were displayed in the 6 and 12 h p.i. RNA samples, but not in mock-infected Sf9 cells. This indicated that AcMNPV-miR-3 exhibited a number of expressions at 6 and 12 h p.i. in AcMNPV infected Sf9 cells. Furthermore, AcMNPV-miR-3 expression levels were tested by using stem-loop qRT-PCR in AcMNPV infected (MOI of 10) Sf9 cells at different time points (0, 6, 12, 24, and 48 h p.i.). The results in Fig. 2B showed that AcMNPV-miR-3 could be initially detected at 6 h p.i. and reached a maximum level around 12 h p.i., which were consistent with the northern blot results.

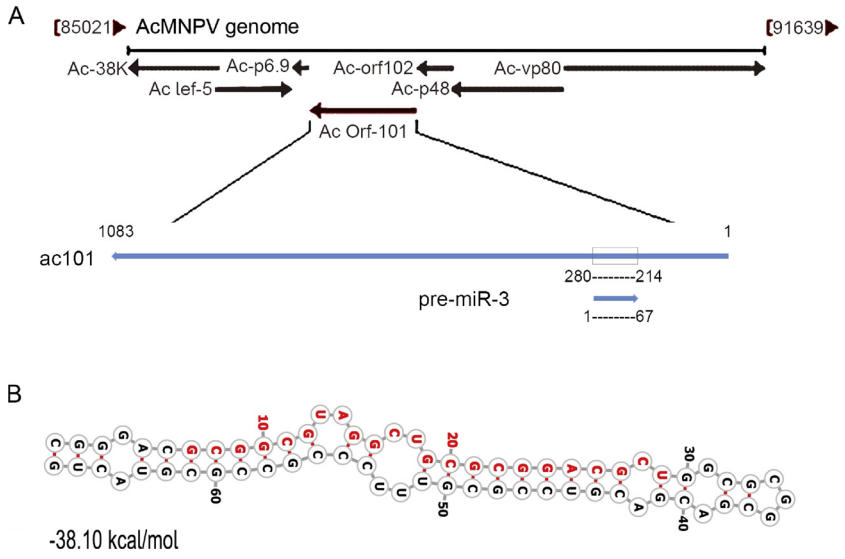

Fig. 1. Schematic representation of AcMNPV-miR-3. (A). The relative position of pre-miR-3 in AcMNPV genome. (B) RNAfold web server was used to predict the hairpin structure of precursor miR-3 with MFE of -38.10 kcal/mol. The predicted mature miR-3 sequence is depicted in red.

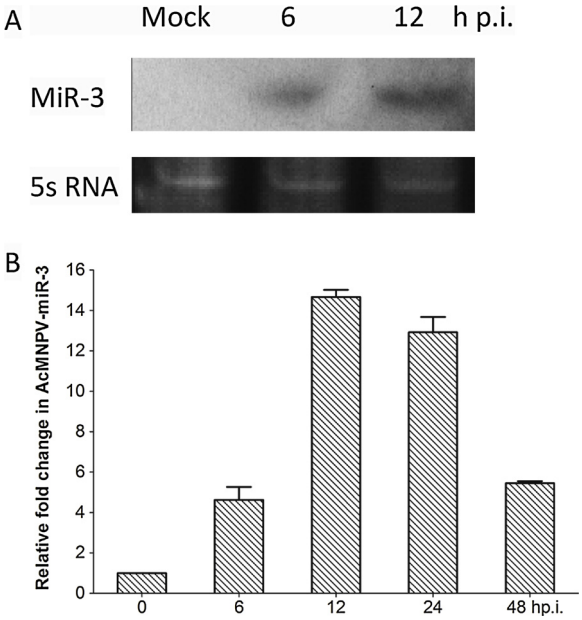

Fig. 2. Experimental validation of AcMNPV-miR-3. A), Northern blot validation of AcMNPV-miR-3. Total RNA was isolated from the following: lane 1, mock-infected Sf9 cells; lane 2, AcMNPV infected Sf9 cells at 6 h p.i.; lane 3, AcMNPV infected Sf9 cells at 12 h p.i.; 5S rRNA was used as a loading control. Please see Fig. 2S in the Supplementary Material for full blot image. B), Relative fold changes in miR-3 expression levels investigated by qRT-PCR. The expression level at each time point was normalized against the 5S rRNA. RNA samples were isolated from Sf9 cells at 0, 6, 12, 24,and 48 h p.i. (10MOI). 5S rRNA was used as an endogenous control, and the 2-ΔΔCt method ($P < 0.005$) was used to calculate the expression level of each sample. The Cq value of no template controls (NTCs) > 40. Each reaction was performed in triplicate four independent times. Error bars represent the standard deviation.

3.3. AcMNPV-miR-3 target genes prediction and validation

To investigate the function and the underlying mechanism of miR-3 in AcMNPV infection, the potential candidate target viral genes of miR-3 were predicted by screening the AcMNPV genome. The seed sequence of a miRNA is defined as the 2–8 nt region at the 5′ end of the mature miRNA, and complementarity to the miRNA seed sequence appears to be a common principle in target recognition (Lambert et al., 2011; Parker et al., 2009). Herein, seven viral genes (*ac10*, *ac23*, *ac25*, *ac86*, *ac98*, *ac101*, and *ac126*) were predicted to be the potential targets (see Supplementary Table 2). The details of the molecular interactions between miR-3 and its targets were depicted in Fig. 3. The results showed that the binding of the miR-3 and the target mRNA was restricted to mainly the 5′ end of the miR-3. Mutations of the seed-matched target binding sites of the miR-3 were established to study whether the mutations could impact the miRNA/tartet binding. The putative targets and their mutations were cloned into the psiCHECK2 vector for luciferase reporter assay. The map of psiCHECK2 plasmid was shown in the Fig. 4A, and the binding site sequences of the putative targets and their mutations (mutated at the putative binding sites of miR-3 seed region) were shown in Fig. 4B. Owing to the complication of the associated molecular interaction between viral miRNAs and their host genes, the HEK293 cell line was utilized as an unrelated cell line to check the possible miRNA targets to avoid unknown virus-host interactions.

Reporter gene expression assay demonstrated that miR-3 mimic robustly reduced *ac23*, *ac25*, *ac86*, *ac98*, and *ac101* reporter gene expression, and the Rluc/Fluc values were 0.78 (*ac23*), 0.69 (*ac25*), 0.67 (*ac86*), 0.65 (*ac98*), and 0.32 (*ac101*) (see in Fig. 4C). The mutation reporter at the seed complementary sites of *ac23*, *ac25*, *ac86*, *ac98*, and *ac101* rescued the repression by the miR-3 mimics, while the *ac101* reporter was only partly rescued. In contrast, miR-3 mimic had no effect on the A3 reporter. Nevertheless, ac10 and ac126 reporter gene expression levels were slightly suppressed, with the Rluc/Fluc values being 0.88 (*ac10*) and 0.85 (*ac126*). These data suggested that *ac23*, *ac25*, *ac86*, *ac98*, and *ac101* reporters were suppressed by miR-3 via directly binding to the CDS segments, and the miRNA-mRNA interactions based mainly on the seed region match.

3.4. The down regulation of ac101 caused by miR-3 mimic

As mentioned above, the viral gene *ac101* had a perfectly matched binding site to miR-3, and the dual luciferase reporter assay showed that the presence of the miR-3 leads to a repression of the *ac101* reporter activities. The *ac101* reporter activities were sharply repressed (to 32%) by the miR-3. It would be very interesting to determine whether and how miR-3 regulates *ac101* gene expression in AcMNPV-infected Sf9 cells. It has been reported that some miRNAs which have a completely complementary binding site in the target gene CDS region would cause a cleavage of the target mRNA if both are temporally co-expressed (Park and Shin, 2014; Sullivan et al., 2009). To determine

```
miR-3: 3' tcGCAGGCGCGTCGGATGCGGCg 5'
            |||::|  ::|  |||||||
ac10: 5' ttCGTTTGACTGG--TACGCCGt 3'

miR-3: 3' tcGCA-GGCGCG-TCGGATGCGGCg 5'
           |||  :|:|| | ::|||||||
ac25: 5' ggCGTAATGTGCTATTTTACGCCGt 3'

miR-3: 3' tcGCAGGCGCG----TCG--GATGCGGCg 5'
           :||:| ||:    |||   |||||||
ac98: 5' caTGTTCTCGTTTTAAGCGAGTACGCCGa 3'

miR-3: 3' tcgcaGGCG-CGTCGGATGCGGCg 5'
              |||: |:|  ||||||||
ac126: 5' gattgCCGTGGTAAACTACGCCGa 3'

miR-3:  3' tcGCAGGCG-CGT-CGGATGCGGCg 5'
           :| |||:  || |::|||||||
ac23:  5' cgTGACCGTATCACGTTTACGCCGa 3'

miR-3: 3' tcgcaggcGCGTCGGATGCGGCg 5'
             |||| | |||||||
ac86: 5' ttaacagcCGCA-CGTACGCCGt 3'

miR-3: 3' tcGCAGGCGCGTCGGATGCGGCg 5'
          ||||||||||||||||||||
ac101: 5' agCGTCCGCGCAGCCTACGCCGc 3'
```

Fig. 3. Pairing schemes of AcMNPV-miR-3 and its predicted targets. As predicted, the miR-3 is targeting to the CDS of the *ac10*, *ac23*, *ac25*, *ac86*, *ac98*, *ac101*, and *ac126* genes. The underline shows the seed region of miR-3.

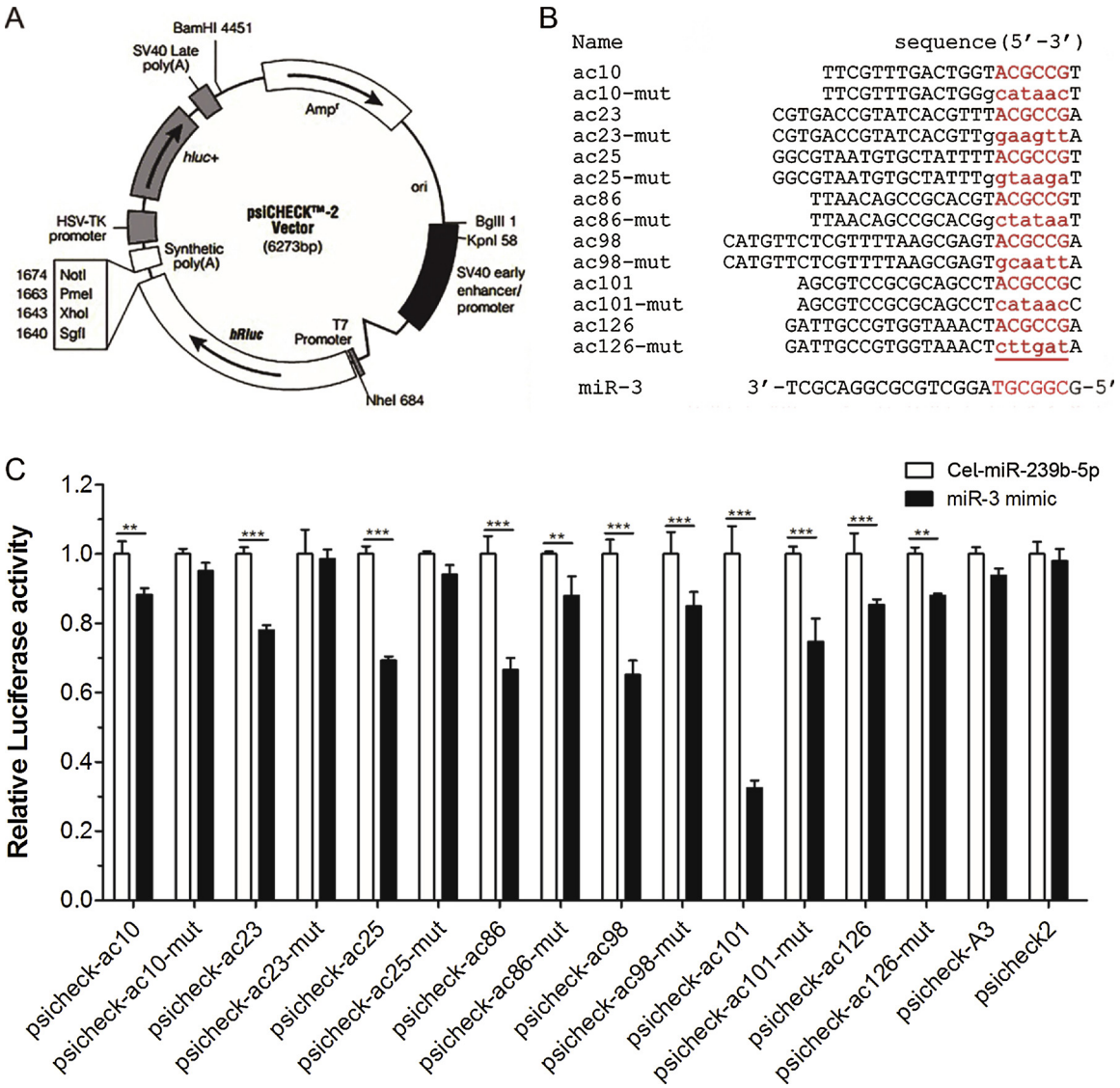

Fig. 4. Target validation for miR-3 by the dual-luciferase reporter assay. (A) Map of the psiCHECK2 vector. (B) The sequences of viral target genes predicted the binding site and their mutations. *Bombyx mori* A3 was used as an unrelated target. The AcMNPV-miR-3 seed region binding sites are marked in red, and the mutated part is highlighted. (C) Relative Rluc/Fluc activity of the AcMNPV-miR-3 predicted target *ac10*, *ac23*, *ac25*, *ac86*, *ac98*, *ac101*, and *ac126*. Dual-luciferase assays were carried out in an HEK293 cell line cotransducted by miRNA mimic and reporter gene vectors, using firefly luciferase as an endogenous control. The Cel-miR-239b-5p mimic was used as a negative control. Rluc/Fluc relative activities were finally normalized to the Rluc/Fluc values for the cells transfected by psiCHECK2. All graphs show the mean values of three independent experiments performed in triplicate. Error bars show the SD (n = 3). **: $P < 0.01$. ***: $P < 0.001$.

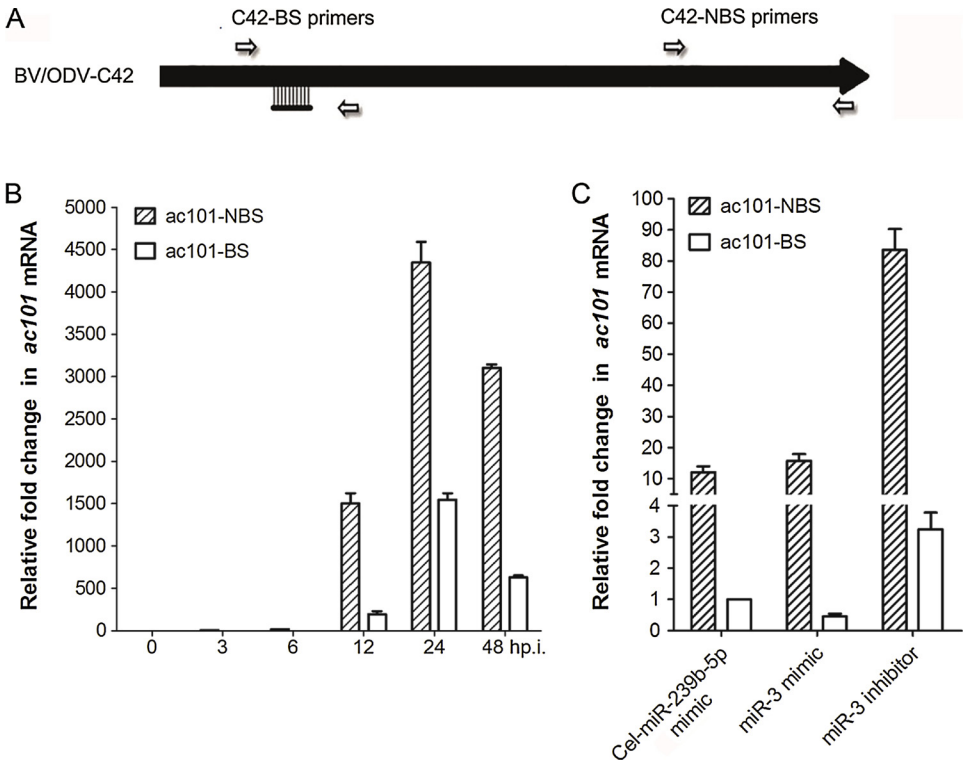

Fig. 5. qRT-PCR analysis determining the regulation of *ac101* mRNA expression levels by AcMNPV-miR-3. (A) Primer pairs used to amplify *ac101* mRNA different regions, one including and the other excluding the AcMNPV-miR-3 binding site. (B) *ac101* mRNA levels at different time points in Sf9 cells infected with AcMNPV, showing the much higher mRNA levels detected by the ac101-NBS primers (hatched columns) compared to that detected by the ac101-BS primers (white columns), with evidence of *ac101* mRNA cleavage at the miR-3 binding site. Total RNAs were extracted from AcMNPV-infected Sf9 cells at the designated time points. The expression level of each sample was normalized against that at 0 h p.i. amplified using each pair of the primers. (C) *ac101* mRNA relative levels at 24 h p.i. in AcMNPV-infected Sf9 cells transfected with the AcMNPV-miR-3 mimic, AcMNPV-miR-3 inhibitor, and Cel-miR-239b-5p mimic (negative control), respectively, showing further down-regulation of *ac101* (more cleavages, white columns) by the miR-3 mimic and the suppression of the down-regulation by the miR-3 inhibitor. It is worth emphasizing that miR-3 mimic did not affect ac101-NBS level (hatched columns), while miR-3 inhibitor increased ac101-NBS level by 9-fold. Total RNA was isolated at 24 h p.i. for each sample. The expression level in each sample was normalized to the Cel-miR-239b-5p mimic. 5S rRNA was used as an endogenous control, and the $2^{-\Delta\Delta Ct}$ method ($P < 0.005$) was used to calculate the expression level of each sample. The $C_q$value of no template controls (NTCs) > 40. Each reaction was performed in triplicate fourindependent times. Error bars represent the standard deviation.

whether miR-3 guided a cleavage of *ac101* mRNA around the binding site, qRT-PCR was performed by using two different pairs of primers (Fig. 5A) designed to amplify different regions of *ac101*, named ac101-BS (binding site, the amplification includes the binding site) and ac101-NBS (non binding site, the amplification excludes the binding site). Ac101-BS primers were designed to amplify the ac101 cDNA encompassing the intact AcMNPV-miR-3 binding site, which reveals the relative amount of ac101 mRNA not cleaved or decayed at the AcMNPV-miR-3 binding site. While, ac101-NBS primers were designed to amplify the 3′ region of ac101 excluding the AcMNPV-miR-3 binding site, representing the total transcribed mRNA level. Therefore, if miR-3 guided cleavage occurred, fewer products amplified by ac101-BS primers would be expected compared to those amplified by ac101-NBS primers.

At first, *ac101* mRNA levels were detected in wild type AcMNPV infected Sf9 cells at different time points post infection. Mock-infected (control) and AcMNPV-infected (MOI of 10) Sf9 cells at 6, 12, 24, and 48 h p.i. samples were harvested for total RNA extraction and qRT-PCR detection. As shown in Fig. 5B, mRNA levels amplified by primer-BS (white column), representing the mRNA level after cleavage or decay from the 5′-terminus onward, were significantly lower than those amplified by primer-NBS (hatched column), representing the total transcribed mRNA level at 24 h p.i. As shown in Fig. 5B, the products amplified by ac101-BS primers (white column) showed significantly less than that amplified by ac101-NBS primers (hatched column) at each time point. As the ac101-BS primers amplification representing the *ac101* mRNA levels after cleavage or decay from the 5′-terminal onward, the results showed that the *ac101* mRNA was cleaved at the expected region.

To determine whether the cleavage was associated with miR-3, the miR-3 mimic and miR-3 inhibitor were synthesized and transfected into AcMNPV infected Sf9 cells for disrupting the miRNA-targets interaction. If a higher level of miR-3 or treatment with miR-3 led to a further lowered primer-BS mRNA level, then the decreased primer-BS mRNA level was related to miR-3 or cleavage occurred and was guided by miR-3. Total RNA samples were extracted from Sf9 cells infected with AcMNPV (MOI of 10) 8 h after transducted with the AcMNPV-miR-3 mimic, AcMNPV-miR-3 inhibitor, or Cel-miR-239b-5p mimic. Then, *ac101* mRNA levels in the three groups of Sf9 cells were tested (Fig. 5C). The results showed in Fig. 6C confirmed that *ac101* mRNA level was related to the miR-3 abundance in AcMNPV infected Sf9 cells. As shown in Fig. 6C, compared to the Cel-miR-239b-5p mimic treatment (mock control), miR-3 mimic treatment led to decreased primer-BS amplification by 50% (white column), indicating that a higher level of miR-3 further decreased the copy number of *ac101* mRNA with whole length,

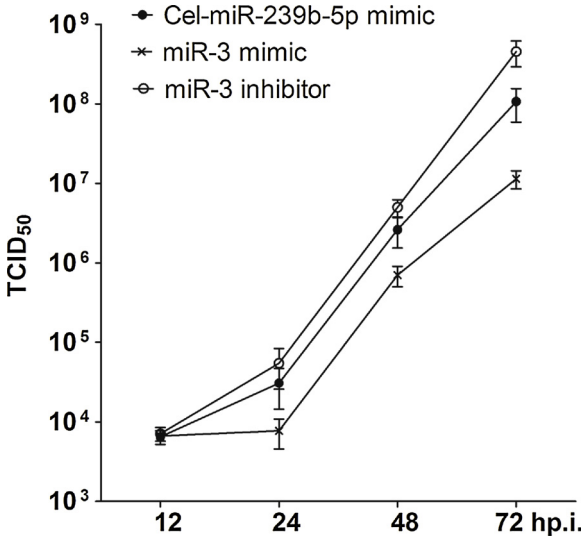

Fig. 6. $TCID_{50}$ end-point dilution assay. The effect of the AcMNPV-miR-3 mimic on the BV titer, showing inhibition of the BV titer by AcMNPV-miR-3. Sf9 cells were infected with AcMNPV (MOI of 1) eight hours after transfection with the miR-3 mimic, miR-3 inhibitor, or cel-miR-239b-5p mimic, respectively.

i.e., miR-3 guided the cleavage of *ac101* mRNA. By contrast, the miR-3 mimic treatment did not reduce the primer-NBS mRNA level (the hatched column) compared with the Cel-miR-239b-5p mimic treatment (mock control), indicating that miR-3 mimic (mature miR-3) treatment would not further suppress ac101 mRNA transcription. These above confirmed that miR-3 guided a cleavage of *ac101* at the 5′-terminal onward of mRNA.

Furthermore, Fig. 6C also shows that miR-3 inhibitor treatment increased the *ac101* primer-NBS mRNA level (the hatched column) by 9-fold. Since the primer-NBS mRNA level represents the total transcribed amount of *ac101* mRNA at 24 h p.i., the result suggested that inhibiting miR-3 increased *ac101* mRNA accumulation, i.e., miR-3 also regulated *ac101* (with a perfectly matched binding site) by severe suppression of mRNA. It was possible that *ac101* mRNA level was strictly controlled by the miR-3. When the dynamic balance between the *ac101* and miR-3 was disrupted, more miR-3 inducing more *ac101* cleaved at the 5′ end. While miR-3 blockage induced more *ac101* mRNA accumulation but the comparable levels of *ac101* with full length. The result suggests that miR-3 regulated ac101 (with a perfectly matched binding site) not only by cleavage of the mRNA but also by severe control of mRNA accumulation.

3.5. AcMNPV-miR-3 affected BV production

To determine whether AcMNPV-miR-3 affects infectious BV production, a viral growth curve analysis was performed using a TCID50 end-point dilution assay. Sf9 cells were infected with AcMNPV (1 MOI) 8 h after transfected with the miR-3 mimic, miR-3 inhibitor or Cel-miR-239b-5p mimic. The supernatants containing BVs were harvested at 24, 48, and 72 h p.i. for a $TCID_{50}$ end-point dilution assay. As expected, a steady increase in BV production was detected in all three groups. Nevertheless, the miR-3 mimic group exhibited a lower BV titer compared to the Cel-miR-239b-5p mimic and miR-3 inhibitor groups at the 24, 48, and 72 h p.i. time points (Fig. 6). Means that, even with the similar initial titer at 12 h p.i., the infectious BV production was suppressed significantly by excessive miR-3 at 48 and 72 h p.i. These results suggest that miR-3 mimic transfection reduces the infectious BV production in AcMNPV infected Sf9 cells.

3.6. The miR-3 mimic expedited polyhedron formation

To determine whether AcMNPV-miR-3 had any effect on viral morphogenesis, infected Sf9 cells (10 MOI) were analyzed by light microscopy and transmission electron microscopy (TEM). Experimental cells were harvested at 36 h p.i. and 72 h p.i. for TEM analysis, and the OBs were observed by light microscopy. The TEM analysis showed that the typical baculovirus infection symptoms were exhibited in the nuclei of the treated Sf9 cells, that is, there were no discernable morphological effects on capsid size or occlusion size or ODV content among the AcMNPV-miR-3 mimic, miR-3 inhibitor and Cel-miR-239b-5p mimic (negative control) groups at 72 h p.i.

However, we noticed that it was easier to find the polyhedron and net-shaped virogenic stroma inundated with electron-dense rod-shaped nucleocapsids by TEM while the miR-3 mimic were transfected. To verify whether miR-3 affects the polyhedron formation in the infected cells, visual analysis of the cells containing OBs were performed by using a light microscope. The results were calculated based on random evaluations of 1000 cells per group. An increased number of cells that containing distinguishable polyhedra was observed in the cells transfected with the miR-3 mimic compared to that in the miR-3 inhibitor group or Cel-miR-239b-5p mimic group at 36 h p.i. (Fig. 7A). Approximately 36.53% of the evaluated cells contained polyhedra in the miR-3 mimic group at 36 h p.i., while the values were 27.24% in the Cel-miR-239b-5p mimic group and 30.83% in the miR-3 inhibitor group, which were significantly lower than the value of the miR-3 group. At 72 h p.i., all three groups exhibited similar phenotypes. These results indicated that the AcMNPV-miR-3 mimic expedited the formation of polyhedra but did not increase the total polyhedron production.

3.7. The expression of miR-3 in recombinant viruses

For further analysis of the role of miR-3 in AcMNPV infected Sf9 cells, over-expressing and RNA-interfered recombinant viruses were constructed. A recombinant virus $v^{Ac-miR-3-GP}$ containing eight tandem additional copies of AcMNPV-miR-3 precursor downstream of the ie1 promoter was constructed for miR-3 overexpression (Fig. 8A). Meanwhile, miR-3 sponge virus was used as the miR-3 inhibitor to block the endogenous miR-3, as artificial miRNA sponges have been applied to explore miRNA functions in vitro and in vivo (Ebert et al., 2007; Tay et al., 2015). The recombinant virus $v^{Ac\text{-}miR\text{-}3\text{-}sponge\text{-}GP}$ containing multiple tandem miR-3 binding sites with bulges was designed. In addition, $v^{Ac\text{-}NC\text{-}GP}$ was constructed with a nonrelated stem-loop structure as a negative control, while $v^{Ac\text{-}WT\text{-}GP}$ was used as the non-insertion control. All these constructs were sequenced to check for the correct insertion.

Considering that AcMNPV-miR-3 had been validated to reach a maximum level around 12 h p.i., and the ie1 promoter could drive the transcription at both early and late time, we extracted the RNA from cell samples infected with the recombinant viruses (MOI of 10) at 12 h p.i. to detect the miR-3 expression by qRT-PCR as mentioned above. As shown in Fig. 8B, the miR-3 expression level showed a three-fold increase in $v^{Ac-miR-3-GP}$ infected Sf9 cells compared to that in the $v^{Ac\text{-}NC\text{-}GP}$ and $v^{Ac\text{-}WT\text{-}GP}$ groups. This demonstrated that miR-3 was successfully overexpressed by the multi-copy of pre-miR-3 in Sf9 cells infected with $v^{Ac-miR-3-GP}$ and enabled us to assess the phenotypic changes that occur in the presence of higher levels of miR-3. However, it is worth noticing that the miR-3 expression level in the $v^{Ac\text{-}miR\text{-}3\text{-}sponge\text{-}GP}$ infected Sf9 cells was approximately five-fold of that in $v^{Ac\text{-}NC\text{-}GP}$ group, even higher than that in $v^{Ac\text{-}miR\text{-}3\text{-}GP}$ group, implying a compensation mechanism, producing more miR-3 to counter for the lack of functional miR-3.

To study the functional difference of miR-3 overexpressed in Sf9 cells infected with recombinant virus $v^{Ac-miR-3-GP}$ and $v^{Ac\text{-}miR\text{-}3\text{-}sponge\text{-}GP}$, we monitored the mRNA levels of five target genes experimentally validated above (Fig. 5). The mRNA levels were determined by qRT-PCR in the $v^{Ac-miR-3-GP}$, $v^{Ac\text{-}miR\text{-}3\text{-}sponge\text{-}GP}$, and $v^{Ac\text{-}NC\text{-}GP}$ virus-infected (MOI of 10) Sf9 cells at 24 h p.i., and all the primer pairs were designed to amplify the target gene sequences corresponding to the miR-3 target site. As illustrated in Fig. 9, the *ac25*, *ac86*, and *ac98* were repressed at comparable rates in the $v^{Ac-miR-3-GP}$ group, approximately 50% lower than the $v^{Ac\text{-}NC\text{-}GP}$. While *ac23* was downregulated by as much as 75%, and *ac101* was downregulated by up to 90%, indicating that multi-copies of miR-3 could make for suppression of the target mRNA levels. In $v^{Ac\text{-}miR\text{-}3\text{-}sponge\text{-}GP}$, the mRNA levels of four in five target genes showed little difference compared to the $v^{Ac\text{-}NC\text{-}GP}$, except for *ac101* that was upregulated by 190%, meaning that, miR-3 sponges can block and neutralize the downregulation of targets such as *ac23, ac25*, *ac86*, and *ac98*, but partially offset the *ac101* cleavage induced by the native miR-3. These results indicated that the excessive expression of mature miR-3 in $v^{Ac-miR-3-GP}$ and $v^{Ac\text{-}miR\text{-}3\text{-}sponge\text{-}GP}$ derived from different mechanism and play different roles. This confirmed that miR-3 was a real miRNA and its expression was tightly controlled in AcMNPV infected Sf9 cells.

4. Discussion

In this study, we characterized a miRNA encoded by AcMNPV, AcMNPV-miR-3. This miRNA was detected at 6 h p.i. and reached a maximum expression level at approximately 12 h p.i. Five viral genes were verified to be the targets of miR-3. Among them, *ac101* was perfectly complementary to the mature miR-3, and identified to be the primary target of miR-3. It is generally accepted that miRNAs silence

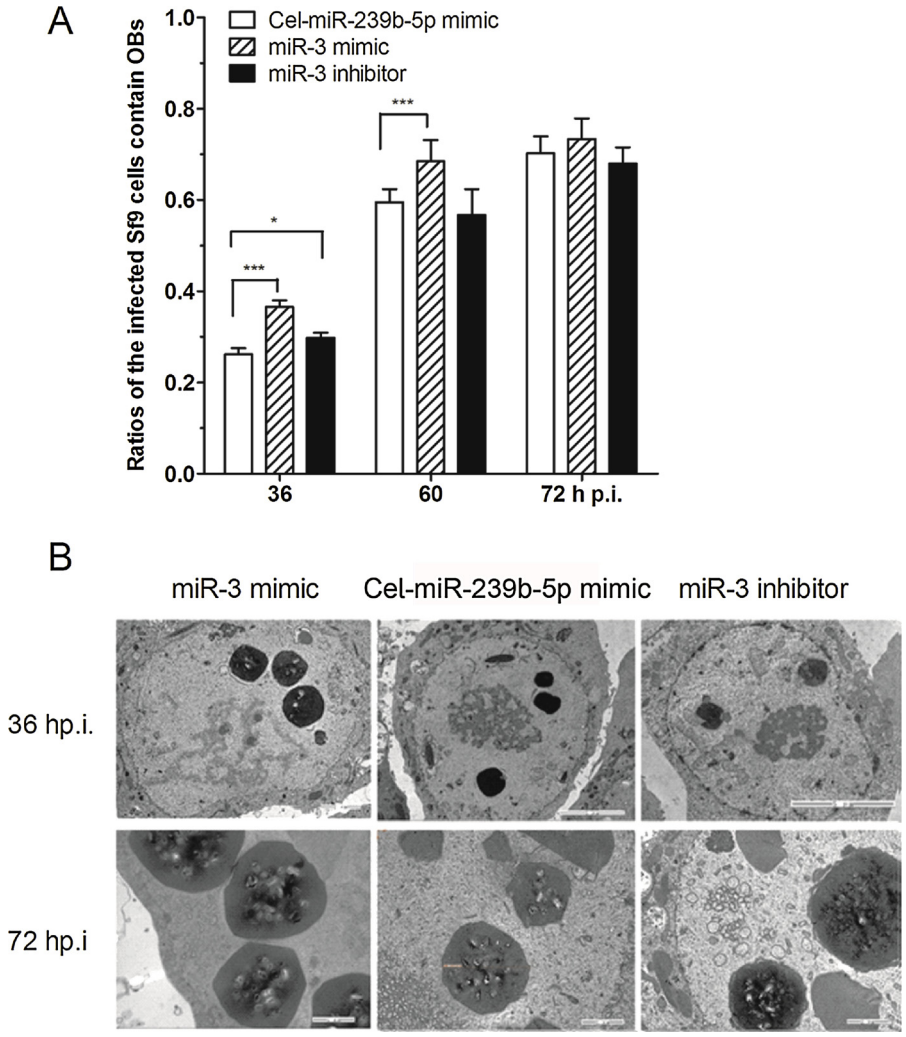

Fig. 7. Analysis of the miR-3 effect on viral morphogenesis. Groups of Sf9 cells were infected with AcMNPV (MOI of 10) 8 h after transfection with the miR-3 mimic, miR-3 inhibitor, and Cel-miR-239b-5p mimic. (A) Percentage of infected Sf9 cells was containing distinguishable polyhedra. A two-way analysis of variance (ANOVA), followed by an LSD (least significant difference) test was used to compare the percentage among three treatment groups. (B) TEM images of three treatment groups of Sf9 cells at 36 and 72 h p.i.

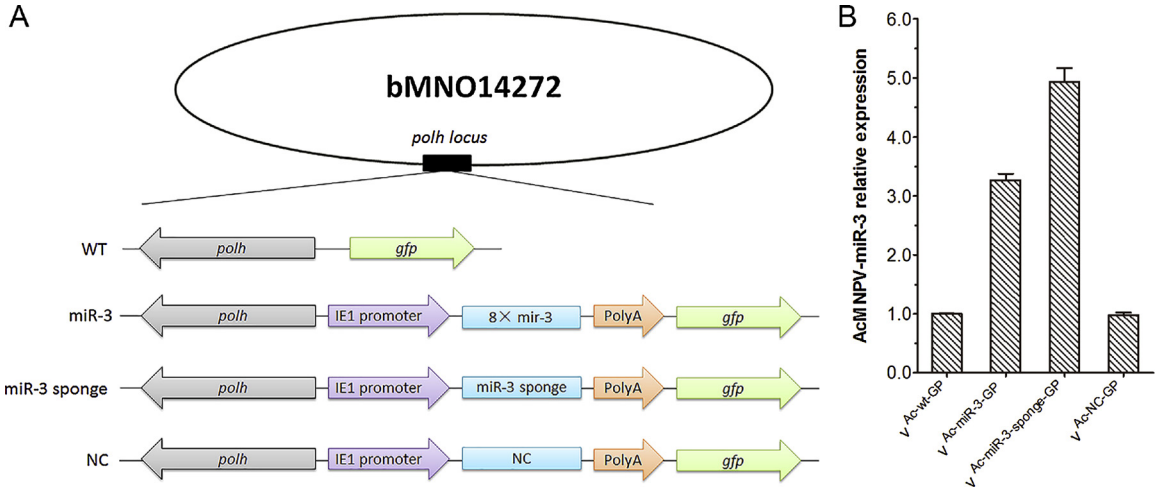

Fig. 8. Construction of $v^{Ac-miR-3-GP}$, $v^{Ac\text{-}miR\text{-}3\text{-}sponge\text{-}GP}$, $v^{Ac\text{-}NC\text{-}GP}$, and $v^{Ac\text{-}WT\text{-}GP}$ bacmids. (A) Schematic diagram of the recombinant viruses. Recombination was conducted using the Bac-to-Bac system. (B) Relative expression of AcMNPV-miR-3 determined by qRT-PCR, showing successful overexpression of AcMNPV-miR-3 in $v^{Ac-miR-3-GP}$ and $v^{Ac\text{-}miR\text{-}3\text{-}sponge\text{-}GP}$ virus infected cells. The columns represent the fold changes in AcMNPV-miR-3 expression normalized to that of 5S rRNA expression. RNA samples were isolated from infected Sf9 cells at 12 h p.i. The quantification cycle value of the no-template control was 40. Each reaction was performed in triplicate in at least three independent experiments. The error bars represent the standard deviations.

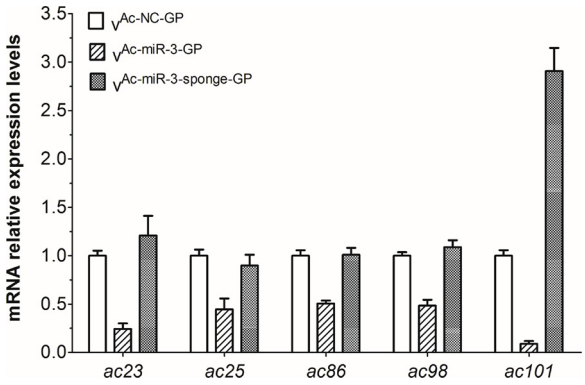

Fig. 9. Regulative expression levels of AcMNPV-miR-3 targets. The mRNA relative levels were tested by qRT-PCR. The columns represent the fold changes in the PCR products. Total RNA samples were isolated from $v^{Ac-miR-3-GP}$, $v^{Ac\text{-}miR\text{-}3\text{-}sponge\text{-}GP}$, and $v^{Ac\text{-}NC\text{-}GP}$ infected Sf9 cells at 24 h p.i. (10 MOI). The RNA level of each target was normalized to that in $v^{Ac\text{-}NC\text{-}GP}$ (each white columns). 5S rRNA was used as a reference and the $2^{-\triangle\triangle CT}$ method was used to calculate the RNA level of each sample. The error bars represent the standard deviations.

gene expression by repressing translation and/or by promoting mRNA decay (Eulalio et al., 2008; Giraldez et al., 2006; Hausser et al., 2013). Some miRNAs that have perfectly match to the complementary binding sites of their target gene would cause target cleavage (Barth et al., 2007; Guo et al., 2005; Hammond et al., 2000; Tuschl et al., 1999; Yekta et al., 2004; Zheng et al., 2012). Our results from qRT-PCR analysis of *ac101* mRNA levels using two different pairs of primers suggested that miR-3 regulated *ac101* by the mRNA cleavage mode and resulted in a suppression of *ac101* mRNA level. Previous studies demonstrated that *ac101* plays essential roles in AcMNPV propagation (Braunagel et al., 2001; Vanarsdall et al., 2007; Wang et al., 2008), whilst recombinant virus with *ac101* knockout produces defective nucleocapsid (Vanarsdall et al., 2007). Nevertheless, in this study, *ac101* depression by excessive miR-3 did not have a noticeable influence on AcMNPV propagation. This may be because miRNA was only a regulatory molecule and it usually had multiple mRNA targets. Nevertheless, more experiments are needed to study more in-depth about the details of miR-3 regulating *ac101* and other targets.

During the viral infection cycle, BVs are produced for the infection of more cells and tissues inside the larvae at the early stage. At the late stage, ODVs are produced for the infection of other larvae in the outside environment. There could be a mechanism regulating genes to switch from the BV production stage to the ODV production stage. The involved factors suppressed BV production and expedited ODV production. AcMNPV-miR-3 might be one of the regulatory factors involved in this mechanism, since transfection of AcMNPV-miR-3 into Sf9 cells inhibited infectious BV production and expedited the formation of polyhedra.

For the further functional study of the miR-3, recombinant viruses were used for stable overexpression of miR-3. It is noteworthy that the AcMNPV-miR-3 expression level in the $v^{Ac-miR-3-sponge-GP}$ was approximately five-fold of that in $v^{Ac\text{-}NC\text{-}GP}$, even more than that in the $v^{Ac\text{-}miR\text{-}3\text{-}GP}$ (three-fold). Nevertheless, the additional mature miR-3 in $v^{Ac-miR-3-sponge-GP}$ has completely different effects on targets regulation when compared to $v^{Ac\text{-}miR\text{-}3\text{-}GP}$. As described previously (Chitwood and Timmermans, 2007; Franco-Zorrilla et al., 2007; Reichel et al., 2015), the expression of miRNAs was always affected by their targets' abundance. These interesting results from the miR-3 sponge may be due to the targets stimulated expression of miR-3. There would have sufficient "sponge RNA" to soak up all the excess miR-3 produced by $v^{Ac-miR-3-sponge-GP}$ for *ac101* was upregulated. Suggesting that miR-3 sponges may work as target mimics to adsorb the mature miR-3 with a higher affinity than the endogenous targets and sequester the miRNA-targets interaction, even stimulate the mature miR-3 expression in a feedback way. Above all, we could speculate that miR-3 expression was strictly controlled by the endogenous pathways. However, given the importance of knowing what works in miR-3 biogenesis, more experiments are certainly needed.

In summary, AcMNPV-miR-3 was a 23-nt long miRNA encoded by AcMNPV, and it can be detected at an early time after AcMNPV infection. Five viral genes were identified to be the targets of miR-3, among them *ac101* is the primary target of miR-3 that can be downregulated by miR-3 via an mRNA cleavage mode. Excessive miR-3 can reduce infectious BV production and accelerated ODV production. In conclusion, miR-3 is a potential regulator in AcMNPV infection and BV/ODV switch. While the more functional mechanism of AcMNPV-miR-3 still needs to be further study.

Acknowledgments

This work was supported by the National Science Foundation of China [grant number 31872024] and the Guangzhou Science and Technology Project [grant number 201707020003].

Appendix A. Supplementary data

Supplementary material related to this article can be found, in the online version, at doi:https://doi.org/10.1016/j.virusres.2019.05.004.

References

Agarwal, S., Vaz, C., Bhattacharya, A., Srinivasan, A., 2010. Prediction of novel precursor miRNAs using a context-sensitive hidden Markov model (CSHMM). BMC Bioinformatics 11 (Suppl. 1), S29.
Bartel, D.P., 2004. MicroRNAs: genomics, biogenesis, mechanism, and function. Cell 116 (2), 281–297.
Barth, S., Pfuhl, T., Mamiani, A., Ehses, C., Roemer, K., Kremmer, E., Jaker, C., Hock, J., Meister, G., Grasser, F.A., 2007. Epstein-Barr virus-encoded microRNA miR-BART2 down-regulates the viral DNA polymerase BALF5. Nucleic Acids Res. 36 (2), 666–675.
Braunagel, S.C., Guidry, P.A., Rosas-Acosta, G., Engelking, L., Summers, M.D., 2001. Identification of BV/ODV-C42, an Autographa californica nucleopolyhedrovirus orf101-encoded structural protein detected in infected-cell complexes with ODV-EC27 and p78/83. J. Virol. 75 (24), 12331–12338.
Chen, C., Ridzon, D.A., Broomer, A.J., Zhou, Z., Lee, D.H., Nguyen, J.T., Barbisin, M., Xu, N.L., Mahuvakar, V.R., Andersen, M.R., Lao, K.Q., Livak, K.J., Guegler, K.J., 2005. Real-time quantification of microRNAs by stem-loop RT-PCR. Nucleic Acids Res. 33 (20), e179.
Chitwood, D.H., Timmermans, M.C., 2007. Target mimics modulate miRNAs. Nat. Genet. 39 (8), 935–936.
Dong, H., Lei, J., Ding, L., Wen, Y., Ju, H., Zhang, X., 2013. MicroRNA: function, detection, and bioanalysis. Chem. Rev. 113 (8), 6207–6233.
Ebert, M.S., Neilson, J.R., Sharp, P.A., 2007. MicroRNA sponges: competitive inhibitors of small RNAs in mammalian cells. Nat. Methods 4 (9), 721–726.
Eulalio, A., Huntzinger, E., Nishihara, T., Rehwinkel, J., Fauser, M., Izaurralde, E., 2008. Deadenylation is a widespread effect of miRNA regulation. RNA 15 (1), 21–32.
Franco-Zorrilla, J.M., Valli, A., Todesco, M., Mateos, I., Puga, M.I., Rubio-Somoza, I., Leyva, A., Weigel, D., García, J.A., Paz-Ares, J., 2007. Target mimicry provides a new mechanism for regulation of microRNA activity. Nat. Genet. 39 (8), 1033–1037.
Giraldez, A.J., Mishima, Y., Rihel, J., Grocock, R.J., Van Dongen, S., Inoue, K., Enright, A.J., Schier, A.F., 2006. Zebrafish MiR-430 promotes deadenylation and clearance of maternal mRNAs. Science 312 (5770), 75–79.
Giudice, A., D'Arena, G., Crispo, A., Tecce, M.F., Nocerino, F., Grimaldi, M., Rotondo, E., D'Ursi, A.M., Scrima, M., Galdiero, M., Ciliberto, G., Capunzo, M., Franci, G., Barbieri, A., Bimonte, S., Montella, M., 2016. Role of viral miRNAs and epigenetic modifications in epstein-barr virus-associated gastric carcinogenesis. Oxid. Med. Cell. Longev. 2016, 6021934.
Grundhoff, A., Sullivan, C.S., Ganem, D., 2006. A combined computational and microarray-based approach identifies novel microRNAs encoded by human gamma-herpesviruses. RNA 12 (5), 733–750.
Guo, H.S., Xie, Q., Fei, J.F., Chua, N.H., 2005. MicroRNA directs mRNA cleavage of the transcription factor NAC1 to downregulate auxin signals for arabidopsis lateral root development. Plant Cell 17 (5), 1376–1386.
Hammond, S.M., Bernstein, E., Beach, D., Hannon, G.J., 2000. An RNA-directed nuclease mediates post-transcriptional gene silencing in Drosophila cells. Nature 404 (6775), 293–296.
Hausser, J., Syed, A.P., Bilen, B., Zavolan, M., 2013. Analysis of CDS-located miRNA target sites suggests that they can effectively inhibit translation. Genome Res. 23 (4), 604–615.
Hussain, M., Asgari, S., 2014. MicroRNAs as mediators of insect host–pathogen interactions and immunity. J. Insect Physiol. 70, 151–158.

Jehle, J.A., Blissard, G.W., Bonning, B.C., Cory, J.S., Herniou, E.A., Rohrmann, G.F., Theilmann, D.A., Thiem, S.M., Vlak, J.M., 2006. On the classification and nomenclature of baculoviruses: a proposal for revision. Arch. Virol. 151 (7), 1257–1266.
Jiang, P., Wu, H., Wang, W., Ma, W., Sun, X., Lu, Z., 2007. MiPred: classification of real and pseudo microRNA precursors using random forest prediction model with combined features. Nucleic Acids Res. 35 (Web Server issue), W339–44.
Kim, S.W., Li, Z., Moore, P.S., Monaghan, A.P., Chang, Y., Nichols, M., John, B., 2010. A sensitive non-radioactive northern blot method to detect small RNAs. Nucleic Acids Res. 38 (7) e98-e98.
Kincaid, R.P., Sullivan, C.S., 2012. Virus-encoded microRNAs: an overview and a look to the future. PLoS Pathog. 8 (12), e1003018.
Lambert, N.J., Gu, S.G., Zahler, A.M., 2011. The conformation of microRNA seed regions in native microRNPs is prearranged for presentation to mRNA targets. Nucleic Acids Res. 39 (11), 4827–4835.
Li, Y., Wang, J., Deng, R., Zhang, Q., Yang, K., Wang, X., 2005. vlf-1 deletion brought AcMNPV to defect in nucleocapsid formation. Virus Genes 31 (3), 275–284.
Li, R., Yu, C., Li, Y., Lam, T.W., Yiu, S.M., Kristiansen, K., Wang, J., 2009. SOAP2: an improved ultrafast tool for short read alignment. Bioinformatics 25 (15), 1966–1967.
Li, K., Wang, Y., Bai, H., Wang, Q., Song, J., Zhou, Y., Wu, C., Chen, X., 2010. The putative pocket protein binding site of Autographa californica nucleopolyhedrovirus BV/ODV-C42 is required for virus-induced nuclear actin polymerization. J. Virol. 84 (15), 7857–7868.
Llave, C., Xie, Z., Kasschau, K.D., Carrington, J.C., 2002. Cleavage of scarecrow-like mRNA targets directed by a class of Arabidopsis miRNA. Science 297 (5589), 2053–2056.
Lo, H.R., Chao, Y.C., 2004. Rapid titer determination of baculovirus by quantitative real-time polymerase chain reaction. Biotechnol. Prog. 20 (1), 354–360.
Miranda, K.C., Huynh, T., Tay, Y., Ang, Y.S., Tam, W.L., Thomson, A.M., Lim, B., Rigoutsos, I., 2006. A pattern-based method for the identification of MicroRNA binding sites and their corresponding heteroduplexes. Cell 126 (6), 1203–1217.
Park, J.H., Shin, C., 2014. MicroRNA-directed cleavage of targets: mechanism and experimental approaches. BMB Rep. 47 (8), 417–423.
Parker, J.S., Parizotto, E.A., Wang, M., Roe, S.M., Barford, D., 2009. Enhancement of the seed-target recognition step in RNA silencing by a PIWI/MID domain protein. Mol. Cell 33 (2), 204–214.
Reichel, M., Li, Y., Li, J., Millar, A.A., 2015. Inhibiting plant microRNA activity: molecular SPONGEs, target MIMICs and STTMs all display variable efficacies against target microRNAs. Plant Biotechnol. J. 13 (7), 915–926.
Rohrmann, G.F., 2013. Baculovirus Molecular Biology. National Center for Biotechnology Information (US), Bethesda (MD).
Singh, J., Singh, C.P., Bhavani, A., Nagaraju, J., 2010. Discovering microRNAs from Bombyx mori nucleopolyhedrosis virus. Virology 407 (1), 120–128.
Singh, C.P., Singh, J., Nagaraju, J., 2012. A baculovirus-encoded microRNA (miRNA) suppresses its host miRNA biogenesis by regulating the exportin-5 Cofactor Ran. J. Virol. 86 (15), 7867–7879.
Singh, C.P., Singh, J., Nagaraju, J., 2014. bmnpv-miR-3 facilitates BmNPV infection by modulating the expression of viral P6.9 and other late genes in Bombyx mori. Insect Biochem. Mol. Biol. 49, 59–69.
Skalsky, R.L., Cullen, B.R., 2010. Viruses, microRNAs, and host interactions. Annu. Rev. Microbiol. 64 (1), 123–141.
Sullivan, C.S., Sung, C.K., Pack, C.D., Grundhoff, A., Lukacher, A.E., Benjamin, T.L., Ganem, D., 2009. Murine polyomavirus encodes a microRNA that cleaves early RNA transcripts but is not essential for experimental infection. Virology 387 (1), 157–167.
Svoboda, P., 2015. A toolbox for miRNA analysis. FEBS Lett. 589 (14), 1694–1701.
Tay, F.C., Lim, J.K., Zhu, H., Hin, L.C., Wang, S., 2015. Using artificial microRNA sponges to achieve microRNA loss-of-function in cancer cells. Adv. Drug Deliv. Rev. 81, 117–127.
Tuschl, T., Zamore, P.D., Lehmann, R., Bartel, D.P., Sharp, P.A., 1999. Targeted mRNA degradation by double-stranded RNA in vitro. Genes Dev. 13 (24), 3191–3197.
Vanarsdall, A.L., Pearson, M.N., Rohrmann, G.F., 2007. Characterization of baculovirus constructs lacking either the Ac 101, Ac 142, or the Ac 144 open reading frame. Virology 367 (1), 187–195.
Wang, Y., Wang, Q., Liang, C., Song, J., Li, N., Shi, H., Chen, X., 2008. Autographa californica multiple nucleopolyhedrovirus nucleocapsid protein BV/ODV-C42 mediates the nuclear entry of P78/83. J. Virol. 82 (9), 4554–4561.
Wang, Y., Zhang, Y., Han, S., Hu, X., Zhou, Y., Mu, J., Pei, R., Wu, C., Chen, X., 2015. Identification of a novel regulatory sequence of actin nucleation promoting factor encoded by Autographa californica multiple nucleopolyhedrovirus. J. Biol. Chem. 290 (15), 9533–9541.
Yekta, S., Shih, I.H., Bartel, D.P., 2004. MicroRNA-directed cleavage of HOXB8 mRNA. Science 304 (5670), 594–596.
Zhang, Y., Hu, X., Mu, J., Hu, Y., Zhou, Y., Zhao, H., Wu, C., Pei, R., Chen, J., Chen, X., Wang, Y., 2018. Ac102 participates in nuclear actin polymerization by modulating BV/ODV-C42 ubiquitination during Autographa californica multiple nucleopolyhedrovirus infection. J. Virol. 92 (12).
Zheng, Y., Li, Y.F., Sunkar, R., Zhang, W., 2012. SeqTar: an effective method for identifying microRNA guided cleavage sites from degradome of polyadenylated transcripts in plants. Nucleic Acids Res. 40 (4) e28-e28.
Zhu, M., Wang, J., Deng, R., Xiong, P., Liang, H., Wang, X., 2013. A MicroRNA encoded by Autographa californica nucleopolyhedrovirus regulates expression of viral gene ODV-E25. J. Virol. 87 (23), 13029–13034.
Zhu, M., Wang, J., Deng, R., Wang, X., 2016. Functional regulation of an Autographa californica nucleopolyhedrovirus-encoded MicroRNA, AcMNPV-miR-1, in Baculovirus Replication. J. Virol. 90 (14), 6526–6537.